2014 IEEE International Conference on Robotics and Automation, Hong Kong, China, June, 2014.

Control Strategy for Whole-Arm Manipulation of a Polygonal Object by Considering the Estimated Bounds of Frictional Coefficient

Masahito Yashima and Tasuku Yamawaki

***Abstract*— The present paper discusses a planning and control strategy for robotic whole-arm manipulation of a slippery polygonal object by taking into account the estimated bounds of the frictional coefficient. In this study, randomized planning methods are first proposed in order to generate contact state transitions. Second, a novel control strategy that can switch manipulation between quasi-static, dynamic, and caging manipulation modes is proposed. Solving the forward dynamics problem, which is formulated as a complementarity problem, generates the desired trajectory and thus ensures that undesirable contact modes do not occur within the estimated bounds of the frictional coefficient. The validity of the proposed methods is then demonstrated through simulations and experiments.**

I. Introduction

Robotic hands are currently in widespread use for automated assembly and manufacturing tasks. However, many challenges must be resolved before they can be used in other industrial applications. For example, a number of important tasks in assembly and manufacturing require objects to be rotated into different orientations. In such cases, fingertip manipulation, which requires repeated grasping and releasing of objects when large reorientations are necessary, is traditionally used. However, this method is somewhat unreliable because it is easily affected by uncertainties. In contrast, whole-arm manipulation, which encloses objects with multiple fingers and palms, has the potential ability to carry out large reorientations continuously and robustly by allowing the objects to slip on the surface of the fingers and fixed palms. However, most studies to date have focused primarily on *power grasps* that attain the immobilization of objects by preventing sliding within the robotic hand grasp when external forces are applied [8], [20].

The present paper addresses the problem of manipulating a polygonal object from an initial configuration to a target configuration by using fingers and a fixed palm (environment) with frictional contacts, as shown in Fig. 1. Since large reorientations of the polygonal object are performed relative to the fingers and palm, changes in the contact states (such as the vertex-edge and edge-edge contacts) occur among all of the bodies in the system, which causes several problems with planning and control. Examples of such problems include (i) the need to change the kinematics and mechanics of the manipulation system frequently in accordance with contact state transitions; (ii) the potential for incurring undesirable rolling, sliding, and breaking contact modes in the presence of friction, unless proper joint torques are planned by taking into account the uncertainties of frictional coefficients and the dynamic validity of the manipulation for the applied joint torque.

M. Yashima and T. Yamawaki are with the Dept. of Mechanical Systems Engineering, National Defense Academy of Japan, 1-10-20 Hashirimizu, Yokosuka, Japan. {yashima, yamawaki} @ nda.ac.jp

A. Related research

Related studies on whole-arm manipulation or in-hand manipulation are as follows: Song, Yashima, and Kumar [10] proposed dynamic whole-arm manipulation simulators that can deal with inconsistencies in the forward dynamics problem. Yashima et al. [17] proposed a planning algorithm for the in-hand manipulation of three-dimensional (3D) smooth objects based on randomized techniques. Harada and Kaneko [3] discussed acceptable conditions for the manipulation of an envelope family. Watanabe [15] discussed a manipulation method that allows rolling and sliding contacts based on an analysis of closure properties. However, these research efforts dealt with local manipulation of smooth objects without addressing contact state transitions. In order to achieve large reorientation of non-smooth objects, it is necessary to carry out global manipulation planning by considering the transition of contact states between the objects, fingers, and the environment. In contrast, Trinkle et al. [13], [14] discussed the quasi-static manipulation of polygonal objects with contact state transitions. Their research implied that it is possible to plan a global manipulation with or without friction by building a contact formation tree joining first-order stability cells. However, they did not present a detailed planning tree creation algorithm that would ensure undesirable contact modes did not occur in the presence of friction, which is what motivates our investigation of these issues.

There are a variety of other manipulation studies that relate to this paper. Manipulation planning of polygonal objects based on a quasi-static model was discussed in [6], [18]. However, the quasi-static manipulations they examined are inapplicable to a variety of tasks. In an attempt to remove such limitations, dynamic manipulations that use gravitational, inertial, and centrifugal forces as driving forces to control object motions were discussed in [5], [7], [11]. However, since manipulation performance is significantly affected by modeling errors, dynamic manipulations may not be used as a primary manipulation method. Caging manipulations, in which fingers restrict an object to a bounded space, were proposed in [9], [19]. However, in that study, motions were limited to a horizontal plane and object manipulation using external forces, while maintaining caging, was not discussed.

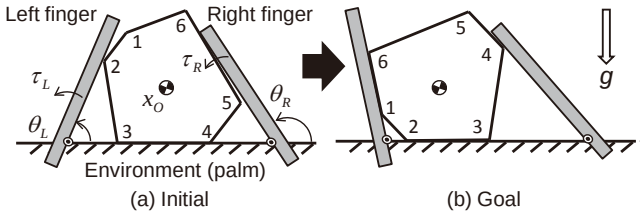

Fig. 1. Initial and goal configurations of whole-arm manipulation

B. Contribution

The main contributions of the present paper are as follows: First, randomized planning for generating contact state transitions for whole-arm manipulations of a slippery polygonal object in frictional contact with the fingers and the environment is proposed. This was accomplished by extending our planning algorithm [16] from frictionless to frictional contact cases. Second, a novel control strategy in the presence of friction that can switch manipulation modes between quasi-static, dynamic, and caging manipulation modes is proposed. As the primary manipulation mode, the desired trajectory that satisfies the quasi-static equilibrium within the estimated bounds of frictional coefficient is generated. If quasi-static manipulation cannot be continued, dynamic manipulation is then performed. Caging manipulation is performed if the gravity force applied to the object can be used to generate a desired rotational manipulation motion. The feasibility of each manipulation mode is verified by solving the forward dynamics problem. This is formulated as a complementarity problem in order to ensure that undesirable contact modes (rolling contacts in this case) do not occur for the applied joint torque.

In the next section, we present the formulation for the quasi-static manipulation with frictional contacts. Section III shows manipulation planning, which is composed of two phases. The first phase obtains a contact state transition graph, while the second phase generates the desired trajectory that can perform the desired contact state transition obtained in the first phase by switching between manipulation modes. In Section IV, the validity of the proposed methods is demonstrated through simulations and experiments. Finally, we present our conclusions and future work.

II. Quasi-static model

A. Assumption

Consider a robotic hand system shown in Fig. 1, which is composed of two one-degree-of-freedom (1-DOF) fingers and an environment. We assume that 1) the object, fingers, and environment are rigid slippery polygons; 2) the coefficient of friction lies between estimated bounds; 3) vertex-to-vertex contact is negligible; 4) the object makes contact with at least one point of each finger and the environment; and 5) each joint is velocity controlled or torque controlled.

B. Basic equations

The kinematics and statics of the robotic hand system are formulated to obtain a quasi-static manipulation model. Assuming that the object makes contact with the hand system at n points of contact, the kinematic constraints can be expressed as follows:

$$\begin{bmatrix} \boldsymbol{G}_n^T & -\boldsymbol{J}_n \end{bmatrix} \begin{bmatrix} \dot{\boldsymbol{x}}_O \\ \dot{\boldsymbol{\theta}} \end{bmatrix} = \boldsymbol{0} \tag{1}$$

where $\boldsymbol{x}_O \in \Re^3$ is the position and orientation of the object, $\boldsymbol{\theta} \in \Re^2$ is the vector of the joint angles, $\boldsymbol{G}_n \in \Re^{3\times n}$ is the normal contact wrench matrix, and $\boldsymbol{J}_n \in \Re^{n\times 2}$ is the normal Jacobian matrix.

The sliding velocity at contact points can be written as follows:

$$\boldsymbol{v}_t = \begin{bmatrix} \boldsymbol{G}_t^T & -\boldsymbol{J}_t \end{bmatrix} \begin{bmatrix} \dot{\boldsymbol{x}}_O \\ \dot{\boldsymbol{\theta}} \end{bmatrix} \tag{2}$$

where $\boldsymbol{v}_t \in \Re^n$ is the vector of the sliding velocities, $\boldsymbol{G}_t \in \Re^{3\times n}$ is the tangential contact wrench matrix, and $\boldsymbol{J}_t \in \Re^{n\times 2}$ is the tangential Jacobian matrix.

If the object is manipulated quasi-statically by the robotic hand, both the object and the hand system must satisfy the following equilibrium equation, which is based on the assumption of Coulomb friction:

$$\begin{bmatrix} \boldsymbol{G}_n + \boldsymbol{G}_{\mu t} \\ -(\boldsymbol{J}_n^T + \boldsymbol{J}_{\mu t}^T) \end{bmatrix} \boldsymbol{f}_n = \begin{bmatrix} -\boldsymbol{g}_O \\ \boldsymbol{g}_h - \boldsymbol{\tau} \end{bmatrix} \tag{3}$$

where $\boldsymbol{f}_n \in \Re^n$ is the normal contact force vector, $\boldsymbol{g}_O \in \Re^3$ is the gravity force applied to the object, $\boldsymbol{\tau} \in \Re^2$ is the joint driving torque vector, $\boldsymbol{g}_h \in \Re^2$ is the joint torque vector induced by gravity, $\boldsymbol{G}_{\mu t} = -\boldsymbol{G}_t \widetilde{\boldsymbol{\mu}}$, $\boldsymbol{J}_{\mu t}^T = -\boldsymbol{J}_t^T \widetilde{\boldsymbol{\mu}}$, $\widetilde{\boldsymbol{\mu}} = \mathrm{diag}[\mu_1 \xi_1, \cdots, \mu_n \xi_n]$, μ_i is the coefficient of friction, $\xi_i = \mathrm{sgn}(v_{ti})$ is the direction of sliding velocity, and $\mathrm{sgn}()$ is the signum function.

C. Formulation for quasi-static manipulation

In order to perform a quasi-static manipulation, the velocity of the object must be uniquely determined for a given velocity of a joint subset. In addition, the remaining finger must apply the joint driving torque needed to satisfy static equilibrium between the object and the hand system [16].

First, consider the velocity kinematics relationships expressed by (1). A square block matrix is extracted from $\begin{bmatrix} \boldsymbol{G}_n^T & -\boldsymbol{J}_n \end{bmatrix}$ by dividing the two fingers into a velocity-controlled finger and a torque-controlled finger. Equation (1) can be rewritten as

$$\begin{bmatrix} \boldsymbol{G}_n^T & -\boldsymbol{J}_{nT} \end{bmatrix} \begin{bmatrix} \dot{\boldsymbol{x}}_O \\ \dot{\theta}_T \end{bmatrix} = \boldsymbol{J}_{nV} \dot{\theta}_V \tag{4}$$

where $\dot{\theta}_V$ and $\dot{\theta}_T$ are the joint velocities of the velocity-controlled finger and torque-controlled finger, and $\boldsymbol{J}_{nV}$ and $\boldsymbol{J}_{nT}$ are the Jacobian matrices corresponding to $\dot{\theta}_V$ and $\dot{\theta}_T$, respectively.

If the matrix $\begin{bmatrix} \boldsymbol{G}_n^T & -\boldsymbol{J}_{nT} \end{bmatrix} \in \Re^{n\times 4}$ in (4) is nonsingular and the Jacobian matrix, $\boldsymbol{J}_{nV}$, is full row rank, then the velocity of the object, $\dot{\boldsymbol{x}}_O$, can be determined uniquely for an arbitrary joint velocity, $\dot{\theta}_V$, of the velocity-controlled finger.

The second condition is that the hand system must maintain quasi-static equilibrium by using the torque-controlled finger to press the object against the environment and the

velocity-controlled finger. This equilibrium can be expressed by extracting the equations of the object and the torque-controlled finger from (3) as follows:

$$\begin{bmatrix} \boldsymbol{G}_n + \boldsymbol{G}_{\mu t} \\ -(\boldsymbol{J}_{nT}^T + \boldsymbol{J}_{\mu tT}^T) \end{bmatrix} \boldsymbol{f}_n = \begin{bmatrix} -\boldsymbol{g}_O \\ g_T - \tau_T \end{bmatrix} \tag{5}$$

$$\boldsymbol{f}_n > \boldsymbol{0} \tag{6}$$

where τ_T and g_T are the joint driving torque and gravity force, and $\boldsymbol{J}_{\mu tT}$ is a submatrix of $\boldsymbol{J}_{\mu t}$, all of which correspond to the torque-controlled finger. The contact force must be compressive, as shown in (6).

If joint driving torque, τ_T, of the torque-controlled finger that satisfies (5) and (6) is found, then the hand system can be maintained in quasi-static equilibrium.

The above formulations for the kinematics and the static equilibrium imply that the joint velocity, $\dot{\theta}_V$, of the velocity-controlled finger and the joint torque, τ_T, of the torque-controlled finger can be regarded as manipulation system inputs. Since the torque-controlled finger and the velocity-controlled finger can perform compliant and non-compliant motions, respectively, a compliant manipulation can be performed by pressing the object against the hand system with the torque-controlled finger in accordance with the non-compliant motion of the velocity-controlled finger.

III. Manipulation planning

A large orientation change of a polygonal object relative to fingers and a fixed environment with frictional contacts will not only generate the contact state changes (such as vertex-edge and edge-edge contacts) among all bodies, it may also cause undesirable contact modes.

The proposed manipulation planning for whole-arm manipulation consists of two phases. The first phase generates a contact state transition graph connecting the initial and goal configuration. This search is performed for a given nominal coefficient of friction within its estimated bounds based on the assumption that all contacts slide. The second phase generates the desired trajectory for the fingers, which can perform the desired contact state transition obtained in the first phase without occurring rolling contacts for any of the frictional coefficients within its bounds. Three manipulations, quasi-static, dynamic, and caging, are applied.

When the object is constrained by the robotic hand system with four sliding points of contact ($n = 4$), the matrix $\begin{bmatrix} \boldsymbol{G}_n^T & -\boldsymbol{J}_{nT} \end{bmatrix}$ in (4) is square. If the conditions for kinematic constraints of quasi-static manipulation mentioned in Section II-C are satisfied, for a given joint velocity, $\dot{\theta}_V$, of the velocity-controlled finger, the velocity of the object may be determined uniquely. We hereafter suppose the manipulation of an object that contacts the hand system at four points.

A. Phase 1: Search for contact state transition

1) Subgoal network: This phase obtains the contact state transition graph connecting the initial and goal configurations using a randomized algorithm, which is very effective for motion planning with a large dimensional search space [17]. This approach constructs a subgoal network based on the generation of subgoals and the connections between those subgoals according to the contact state transitions. The fundamental algorithm is similar to the one for the frictionless case proposed by the authors [16], except that a nominal frictional coefficient within the estimated bounds is given.

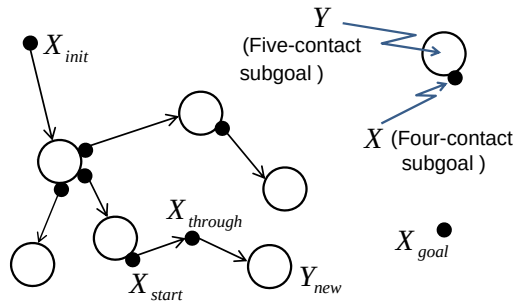

Fig. 2. Generation of subgoals in search space

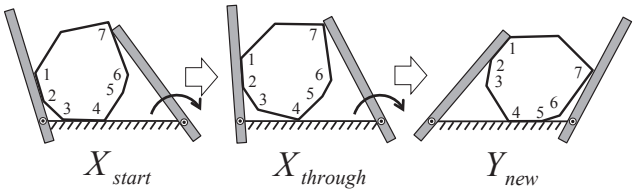

Fig. 3. Overview of subgoal generation. By rotating the right finger clockwise from a four-contact subgoal $\boldsymbol{X}_{start}$, a new five-contact subgoal $\boldsymbol{Y}_{new}$ is generated through $\boldsymbol{X}_{through}$.

All of the subgoals are classified as either four-contact, $\boldsymbol{X}$, or five-contact subgoals, $\boldsymbol{Y}$, as shown in Fig. 2. A pair of subgoals connected by a directed tree is reachable from the parent to child subgoals with either quasi-static manipulation or caging manipulation described in detail in Section III-B.3. The four-contact subgoals attached to identical five-contact subgoals have the same hand and object configuration, but different contact states.

Fig. 3 illustrates the generation of subgoals. First, a five-contact subgoal is randomly selected within the existing subgoals. Then, a start subgoal, $\boldsymbol{X}_{start}$, is generated from the five-contact subgoal by randomly selecting four contact points among the subgoal contact points, as well as the rotational direction of the velocity-controlled finger. Suppose that four contact points, vertex #3 excepted, are selected and that clockwise rotation is assigned to the velocity-controlled right finger. The object rotates clockwise around vertex #4, contacting the environment by moving the right finger while maintaining the current contact state. When the contact state is changed on the way (the right finger is changed from the type-A to the type-B contact [4]), a new subgoal with four contact points, $\boldsymbol{X}_{through}$, is generated. When the object gains five contact points, a new five-contact subgoal, $\boldsymbol{Y}_{new}$, is generated. This process is repeated from the initial configuration, $\boldsymbol{X}_{init}$, to the final configuration, $\boldsymbol{X}_{goal}$.

2) Randomized planning algorithm : The randomized algorithm is described in detail by the MAIN_RANDOM_SEARCH function shown below. Either a velocity-control or a torque-control mode is temporarily

assigned to each finger in this phase.

(Steps 1 and 6) Iterate this process until completing a subgoal network connecting the initial and goal configuration, or until reaching the maximum number of iterations.

(Step 2) A subgoal, $\boldsymbol{Y}_{rand}$, is selected at random from among the existent five-contact subgoals, including the initial subgoal.

(Step 3) If a five-contact subgoal is selected in Step 2, a four-contact subgoal, $\boldsymbol{X}_{start}$, is generated by selecting four contact points at random from the contact points of $\boldsymbol{Y}_{rand}$ without overlapping the existing four-contact subgoals attached to $\boldsymbol{Y}_{rand}$. In addition, the rotational direction of the velocity-controlled finger, dir_joint, is determined randomly.

(Steps 4 and 5) The velocity-controlled finger is moved in the direction of dir_joint with a joint velocity input, $\dot{\theta}_V$, from the configuration of $\boldsymbol{X}_{start}$ in order to generate new subgoals, $\boldsymbol{X}_{through}$ and $\boldsymbol{Y}_{new}$. First, at each time step, the forward kinematics problem is solved to obtain the velocity of the object, $\dot{\boldsymbol{x}}_O$, and the remaining joint velocity, $\dot{\theta}_T$, from (4), and the sliding velocity, $\boldsymbol{v}_T$, from (2), where $\dot{\theta}_V$ with a constant value may be given in this phase. Next, a check is performed to determine whether either quasi-static manipulation or caging manipulation is feasible for a given nominal coefficient of friction, μ^*. Then, a new configuration of the object and fingers at the next time step is calculated. If the object is moved to the final configuration, $\boldsymbol{X}_{goal}$, the search is terminated.

MAIN_RANDOM_SEARCH
1 **for** $i = 1$ to i_{max} **do**
2 $\quad \boldsymbol{Y}_{rand} \leftarrow$ RANDOM_SUBGOAL_Y();
3 $\quad (\boldsymbol{X}_{start}, dir\_joint) \leftarrow$ RANDOM_SUBGOAL_X($\boldsymbol{Y}_{rand}$);
4 $\quad$ NEW_SUBGOAL($\boldsymbol{X}_{start}, \dot{\theta}_V, dir\_joint, \mu^*$);
5 $\quad$ **if** (Object reached $\boldsymbol{X}_{goal}$) **break**;
6 **end for**

B. Phase 2: Trajectory generation

This phase generates trajectories that can perform the desired contact state transition obtained in Phase 1 by taking into consideration the estimated bounds of the frictional coefficient, $\widetilde{\mu} = [\mu_{min},\ \mu_{max}]$. Three manipulations are applied: quasi-static, dynamic, and caging.

1) Quasi-static manipulation: The primary manipulation is quasi-static. For a given coefficient of friction within the estimated bounds $\widetilde{\mu}$, the joint torque of the torque-controlled finger for a quasi-static manipulation is derived. The maximum and minimum joint torques, τ_{max} and τ_{min}, which can satisfy the equilibrium conditions (5) and (6), are obtained by solving the following quadratic programming problem:

$$\begin{aligned} \text{maximize} \quad & \tau_T^2 \quad \left(\text{or} \quad \text{minimize} \ \ \tau_T^2\right) \\ \text{subj. to} \quad & \text{Eqs. (5) and (6)} \\ & -\tau_{limit} \le \tau_T \le \tau_{limit} \end{aligned} \tag{7}$$

where τ_{limit} is the limit torque of the actuators.

The applicable torque range, $\mathcal{T}(\mu) = \{\tau_T |\ \tau_{min} \le \tau_T \le \tau_{max},\ \mu \in \widetilde{\mu}\}$ is bounded by τ_{max} and τ_{min} for a given frictional coefficient μ. Fig. 4 shows the applicable torque ranges, $\mathcal{T}(\mu_{max})$ and $\mathcal{T}(\mu_{min})$, for μ_{max} and μ_{min}, which are drawn as solid and broken curves, respectively. Therefore, the applicable torque range $\mathcal{T}(\widetilde{\mu})$ that satisfies the quasi-static manipulation condition within the bounds of frictional coefficient $\widetilde{\mu} = [\mu_{min},\ \mu_{max}]$ can be described as the intersection of $\mathcal{T}(\mu_{max})$ and $\mathcal{T}(\mu_{min})$, as shown in a hatched region:

$$\mathcal{T}(\widetilde{\mu}) = \mathcal{T}(\mu_{max}) \cap \mathcal{T}(\mu_{min}) \tag{8}$$

Any joint torque in the range $\mathcal{T}(\widetilde{\mu})$ is applicable to the quasi-static manipulation within the estimated bounds of the frictional coefficient, $\widetilde{\mu}$. Here, in order to take modeling errors into consideration, the desired joint torque is generated by adding margin torque, τ_{margin}, to the minimum joint torque, which is shown by a thick line in Fig. 4.

The randomized planning in Phase 1 presumes that sliding occurs at all contacts for the applied joint torque. In order to verify this presumption, the forward dynamics problem is solved at each time step, which can be formulated as a linear complementarity problem (LCP). This approach is widely used to simulate contact phenomena [1], [12]. The forward dynamics problem is detailed in Section III-B.4.

The conditions for the feasibility of the contact state transition with a quasi-static manipulation are as follows:

1) A velocity-controlled finger joint velocity exists that makes it possible to uniquely determine the velocities of an object just before and after contact state transition.
2) A torque-controlled finger joint torque exists that makes it possible to simultaneously satisfy the equilibrium states just before and after contact state transition.

Condition 1 should be satisfied if the contact state transition is obtained in Phase 1 because the forward kinematics problem (4) is solved. However, we should note that Condition 2 is not always satisfied.

2) Dynamic manipulation: When the contact state transition with a quasi-static manipulation is not feasible, dynamic manipulation should be applied. As seen from the intersection, $\mathcal{T}(\widetilde{\mu})$, shown as a hatched region in Fig. 4, this situation occurs when

1) The applicable torque range, $\mathcal{T}(\widetilde{\mu})$, is separated at time $t{=}t_B$.
2) No applicable torque range exists during $t_C \le t \le t_D$.

The desired joint torque of the torque-controlled finger for dynamic manipulation, τ_{dyn}, is determined as follows:

For the first case, a joint torque that exceeds the maximum joint torque, τ_{max}, is applied before $t = t_B$ in order to perform dynamic manipulation by breaking the equilibrium state. For the second case, a constant joint torque is applied during the period of $t_C \le t \le t_D$ in order to perform dynamic manipulation, as shown in Fig. 4.

In order to verify whether the joint torque, τ_{dyn}, causes the contact state transition dynamically with all contacts sliding,

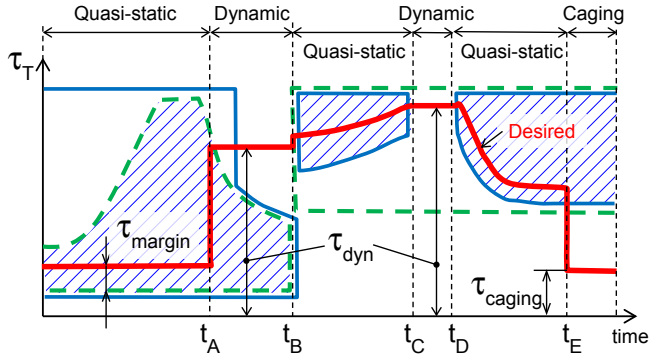

Fig. 4. The torque ranges, $\mathcal{T}(\mu_{max})$ and $\mathcal{T}(\mu_{min})$, are drawn as solid and broken curves, respectively. The intersection $\mathcal{T}(\tilde{\mu})$ is shown as a hatched region. The desired torque trajectory is generated based on manipulation modes.

the forward dynamics problem is solved for both cases in a similar manner to the quasi-static manipulation.

3) Caging manipulation: Caging manipulation, in which the robotic fingers cage the target object, is used to rotate the object around the vertex while maintaining contact with the environment via gravity until another object edge comes into contact with the environment. When the center of gravity of the object crosses the vertex contact normal during the rotation, the manipulation mode can be switched to caging. As shown in Fig. 4, the constant torque τ_{caging}, which is less than the minimum joint torque, is applied in order to ensure that the torque-controlled finger does not prevent the object from moving due to the influence of gravity $(t \geq t_E)$.

4) Formulation of forward dynamics problem: In this section, we will briefly discuss the formulation of the forward dynamics problem of whole-arm manipulation, which is based on the linear complementarity problem using a time-stepping algorithm [12]. Let the superscript l be quantities at time t^l, and h be the time step size. The discrete-time form of the dynamic equations of motion of the object and the torque-controlled finger is given by

$$\boldsymbol{M}\boldsymbol{v}^{l+1} = \boldsymbol{M}\boldsymbol{v}^{l} + \boldsymbol{W}_n^l \boldsymbol{p}_n^{l+1} + \boldsymbol{W}_f^l \boldsymbol{p}_f^{l+1} + h\boldsymbol{u}^l \qquad (9)$$

where $\boldsymbol{M}$ is the inertia matrix, $\boldsymbol{v} = [\dot{\boldsymbol{x}}_O^T,\ \dot{\theta}_T]^T$, $\boldsymbol{W}_n = [\boldsymbol{G}_n^T, -\boldsymbol{J}_{nT}]^T$, $\boldsymbol{W}_f = [\boldsymbol{W}_t, -\boldsymbol{W}_t]$, $\boldsymbol{W}_t = [\boldsymbol{G}_t^T, -\boldsymbol{J}_{tT}]^T$, $\boldsymbol{p}_n \in \Re^n$ and $\boldsymbol{p}_f \in \Re^{2n}$ are normal and friction impulse vectors in the plane, respectively, and $\boldsymbol{u} = [\boldsymbol{g}_0^T, -(g_T + \tau_T)]^T$.

Non-penetration at contact points is enforced by the following complementarity condition:

$$\boldsymbol{0} \leq \boldsymbol{p}_n^{l+1} \perp \boldsymbol{W}_n^T \boldsymbol{v}^{l+1} - \boldsymbol{J}_{nV}\dot{\theta}_V^{l+1} \geq \boldsymbol{0} \qquad (10)$$

where $\perp$ denotes orthogonality.

Coulomb's Law can be written as the following two complementarity conditions in the plane:

$$\boldsymbol{0} \leq \boldsymbol{p}_f^{l+1} \perp \boldsymbol{W}_f^T \boldsymbol{v}^{l+1} - \boldsymbol{J}_{fV}\dot{\theta}_V^{l+1} + \boldsymbol{E}\boldsymbol{\sigma}^{l+1} \geq \boldsymbol{0} \qquad (11)$$

$$\boldsymbol{0} \leq \boldsymbol{\sigma}^{l+1} \perp \boldsymbol{U}\boldsymbol{p}_n^{l+1} - \boldsymbol{E}^T \boldsymbol{p}_f^{l+1} \geq \boldsymbol{0} \qquad (12)$$

where $\boldsymbol{\sigma}$ is the vector of sliding speeds at the contacts. $\boldsymbol{J}_{fV} = [\boldsymbol{J}_{tV}^T, -\boldsymbol{J}_{tV}^T]^T$, $\boldsymbol{E} = [\boldsymbol{E}_n, \boldsymbol{E}_n]^T$, $\boldsymbol{E}_n$ is the $n \times n$ identity matrix, and $\boldsymbol{U} = \mathrm{diag}(\mu_1, \cdots, \mu_n)$.

Putting (9)-(12) together yields the following mixed LCP formulation:

$$\begin{bmatrix} \boldsymbol{0} \\ \boldsymbol{v}_n^{l+1} \\ \boldsymbol{\rho}_f^{l+1} \\ \boldsymbol{s}^{l+1} \end{bmatrix} = \begin{bmatrix} -\boldsymbol{M} & \boldsymbol{W}_n & \boldsymbol{W}_f & \boldsymbol{0} \\ \boldsymbol{W}_n^T & \boldsymbol{0} & \boldsymbol{0} & \boldsymbol{0} \\ \boldsymbol{W}_f^T & \boldsymbol{0} & \boldsymbol{0} & \boldsymbol{E} \\ \boldsymbol{0} & \boldsymbol{U} & -\boldsymbol{E}^T & \boldsymbol{0} \end{bmatrix} \begin{bmatrix} \boldsymbol{v}^{l+1} \\ \boldsymbol{p}_n^{l+1} \\ \boldsymbol{p}_f^{l+1} \\ \boldsymbol{\sigma}^{l+1} \end{bmatrix} + \boldsymbol{b} \qquad (13)$$

$$\boldsymbol{0} \leq \begin{bmatrix} \boldsymbol{v}_n^{l+1} \\ \boldsymbol{\rho}_f^{l+1} \\ \boldsymbol{s}^{l+1} \end{bmatrix} \perp \begin{bmatrix} \boldsymbol{p}_n^{l+1} \\ \boldsymbol{p}_f^{l+1} \\ \boldsymbol{\sigma}^{l+1} \end{bmatrix} \geq \boldsymbol{0} \qquad (14)$$

where $\boldsymbol{b} = \mathrm{col}(\boldsymbol{M}\boldsymbol{v}^l + h\boldsymbol{u}^l, -\boldsymbol{J}_{nV}\dot{\theta}_V^{l+1}, -\boldsymbol{J}_{fV}\dot{\theta}_V^{l+1}, \boldsymbol{0})$, which contains the control inputs, τ_T and $\dot{\theta}_V$. Equations (13) and (14) are solved by using the well-known PATH solver, which is the most robust LCP solver available from [2].

The newly formulated LCP is applicable to the manipulation system that consists of both torque-controlled and velocity-controlled bodies. Its solution yields the estimates of the sliding speed $\boldsymbol{\sigma}$, the normal contact impulse $\boldsymbol{p}_n$, and the velocity of the system at time t^{l+1}. We can determine whether contact i is sliding $(\sigma_i > 0)$, rolling $(\sigma_i = 0)$, or breaking $(p_{ni} > 0)$ when the joint control inputs are applied to the fingers.

5) Control mode: Either a velocity-control or a torque-control mode is assigned to each finger. In contrast with the torque-controlled finger, the velocity-controlled finger (which performs non-compliant motion) may generate jamming and excessive internal forces due to control errors, modeling errors, etc. Therefore, the control modes are assigned based on the object degree of constraint [18] imposed by the velocity-controlled finger and the environment. When comparing two cases in which the velocity control mode is assigned to either the right or left finger, choose the one that has smaller degrees of constraint. This method is not described in detail here due to its length.

6) Trajectory generation algorithm: The trajectory generation algorithm is described by the MAIN_TRAJECTORY function shown below:

(Step 1) Read a series of subgoals connecting the initial and goal configurations obtained in Phase 1.

(Step 2) Set subgoals $\boldsymbol{X}_A$ and $\boldsymbol{X}_B$, which correspond to both ends of the velocity-controlled finger trajectory, where $\boldsymbol{X}_B$ is assigned a subgoal just before the rotational direction of the velocity-controlled finger is reversed. Initially, $\boldsymbol{X}_{init}$ is assigned to $\boldsymbol{X}_A$.

(Step 3) Determine whether the quasi-static transition condition of the contact state mentioned in Section III-B.1 can be satisfied between $\boldsymbol{X}_A$ and $\boldsymbol{X}_B$.

(Step 4) The joint torque, $\tau_T(t)$, of the torque-controlled finger and the joint angle, $\theta_V(t)$, of the velocity-controlled finger between $\boldsymbol{X}_A$ and $\boldsymbol{X}_B$ are calculated at each time step during the time interval ΔT. If the joint torque is not obtained, the planning is then terminated. The details are shown in the next section.

(Steps 5 and 6) If the connected subgoal $\boldsymbol{X}_B$ is equivalent to $\boldsymbol{X}_{goal}$, planning is then successfully terminated. In other

cases, the initial subgoal of the next segment is given, and the process returns to Step 2.

MAIN_TRAJECTORY

1 $(\boldsymbol{X}_{init}, \cdots, \boldsymbol{X}_{goal}) \leftarrow$ Read_Subgoal();
2 $\boldsymbol{X}_B \leftarrow$ Set_BoundarySubgoal $(\boldsymbol{X}_A)$;
3 TransitFlag $\leftarrow$ Check_Transition$(\boldsymbol{X}_A, \boldsymbol{X}_B)$;
4 **for** $t = 0$ to ΔT
$(\tau_T(t),\ \theta_V(t), \text{Flag})$
$\leftarrow$ GET_TRAJ $(\boldsymbol{X}_A, \boldsymbol{X}_B, \Delta T, t, \text{TransitFlag})$;
if (Flag = FALSE) **then** Stop;
end for
5 **if** $(\boldsymbol{X}_B = \boldsymbol{X}_{goal})$ **then** Stop;
6 **else** $\boldsymbol{X}_A \leftarrow$ next subgoal of $\boldsymbol{X}_B$; go to Step 2;

7) Joint trajectory derivation: The GET_TRAJ function, which generates the desired joint torque for the torque-controlled finger and the desired joint angle for the velocity-controlled finger during the segment connecting $\boldsymbol{X}_A$ and $\boldsymbol{X}_B$, is described in detail below:

(Step 1) The trajectory, $\theta_V(t)$, of the velocity-controlled finger between $\boldsymbol{X}_A$ and $\boldsymbol{X}_B$ is calculated. The velocity and acceleration constraints at both ends are zero, and the duration is ΔT.

(Step 2) The forward kinematics problem (4) is solved to obtain the velocity of the object and the remaining joint velocity by giving $\dot{\theta}_V(t)$ obtained in Step 1.

(Steps 3-4) The joint torque, $\tau_{static}(t)$, for a quasi-static manipulation is derived. A determination is made as to whether all contacts slide for the applied torque, $\tau_{static}(t)$, by solving the forward dynamic problem.

(Step 5) If caging manipulation can be applied, the manipulation mode is switched from quasi-static to caging manipulation. The constant joint torque, τ_{caging}, is applied.

(Step 6) When the transition between contact states is not feasible via a quasi-static manipulation, the manipulation modes are switched to dynamic manipulation. A determination is made as to whether specified dynamic manipulation occurs for the applied joint torque, τ_{dyn}, by solving the forward dynamic problem.

(Step 7) A new configuration is calculated by integrating $\dot{\boldsymbol{x}}_O$ with respect to time step h.

(Step 8) Return the calculated joint torque $\tau_T(t)$ and joint angle $\theta_V(t)$.

GET_TRAJ $(\boldsymbol{X}_A, \boldsymbol{X}_B, \Delta T, t, \text{TransitFlag})$
1 $(\theta_V(t), \dot{\theta}_V(t))$
$\leftarrow$ Get_JointTraj $(\boldsymbol{X}_A, \boldsymbol{X}_B, \Delta T, t)$;
2 $(\dot{\boldsymbol{x}}_O(t), \dot{\theta}_T(t)) \leftarrow$ FwdKinematics$(\dot{\theta}_V(t))$;
3 $\tau_{static}(t) \leftarrow$ Get_TorqueQuasiStatic (τ_{margin});
4 **if** (Check_Static $(\tau_{static}(t))$ = TRUE) **then**
$\tau_T(t) \leftarrow \tau_{static}(t)$;
else Flag $\leftarrow$ FALSE;
5 **if** (Check_Caging$(\boldsymbol{x}_O(t))$ = TRUE) **then**
$\tau_T(t) \leftarrow \tau_{caging}$;
6 **if** (TransitFlag = FALSE) **then**
if (Check_Dyn (τ_{dyn}) = TRUE) **then**
$\tau_T(t) \leftarrow \tau_{dyn}$;
else Flag $\leftarrow$ FALSE;
7 $(\boldsymbol{x}_O(t+h), \boldsymbol{\theta}(t+h)) \leftarrow$ NewConfig $(\dot{\boldsymbol{x}}_O(t))$;
8 **return** $(\tau_T(t),\ \theta_V(t),\ \text{Flag})$;

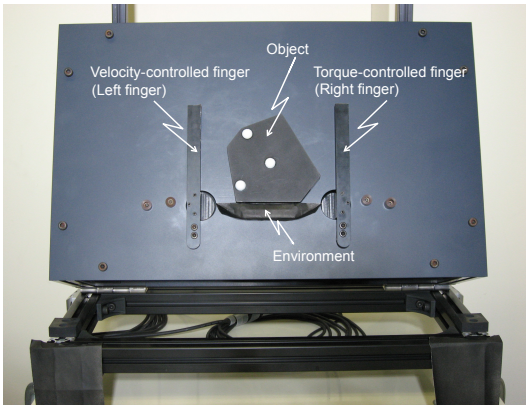

Fig. 5. Two-fingered robotic hand system developed for whole-arm manipulation

IV. Simulations and Experiments

A. Two-fingered robotic hand system

Fig. 5 shows a two-fingered robotic hand system, which was developed for the whole-arm manipulation shown in Fig. 1. The two fingers, each 15 cm in length, are actuated by direct-drive motors. The length between the joint axes of the fingers is 20 cm. A support plane, which is tilted by 15 degrees from the vertical plane, is used to restrict the motion of the object to a planar motion. The friction between bodies is reduced by coating the surface of the fingers and the support plane with Teflon®. The estimated bound of frictional coefficient between bodies is set to $\widetilde{\mu} = [0,\ 0.1]$. The asymmetric hexagonal object was made of plastic resin and has a mass of 353 g.

B. Results of the contact state transition search (Phase 1)

By applying the proposed randomized algorithm, we obtained the desired transition of the contact state for a nominal frictional coefficient, $\mu^* = 0$, as shown in Fig. 6. In this phase, a velocity-control mode is temporarily assigned to the right finger. Each figure shows the configuration of either $\boldsymbol{X}_{start}$ or $\boldsymbol{X}_{through}$. A total of 60 subgoals are generated randomly, from which eleven subgoals were found to connect $\boldsymbol{X}_{init}$ and $\boldsymbol{X}_{goal}$, which correspond to #1 and #11 in Fig. 6. The algorithm was implemented in MATLAB on a 2.6 GHz Xenon 4-core PC, and the computation time averaged 20 min.

C. Results of trajectory generation (Phase 2)

By taking into consideration the estimated bound of the frictional coefficient, we obtained the desired trajectories, as shown in Fig. 7. The torque-control and velocity-control modes are assigned to the right and left fingers, respectively, on the basis of the method mentioned in Section III-B.5.

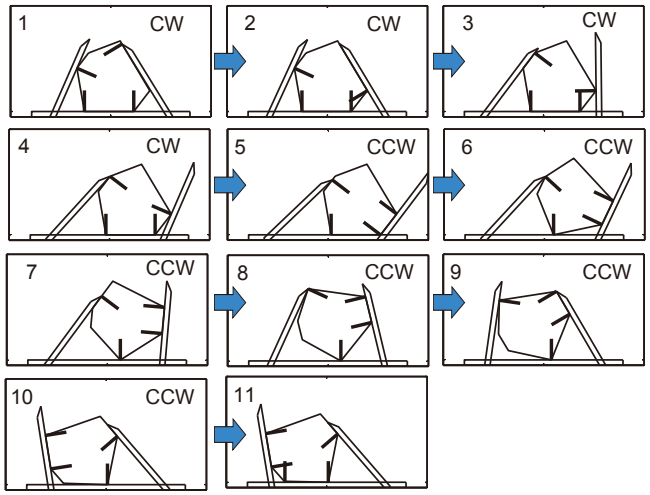

Fig. 6. Contact state transition graph obtained in Phase 1. The rotational directions of the right finger are shown at the top right. The bold lines at the contact points indicate the contact normals.

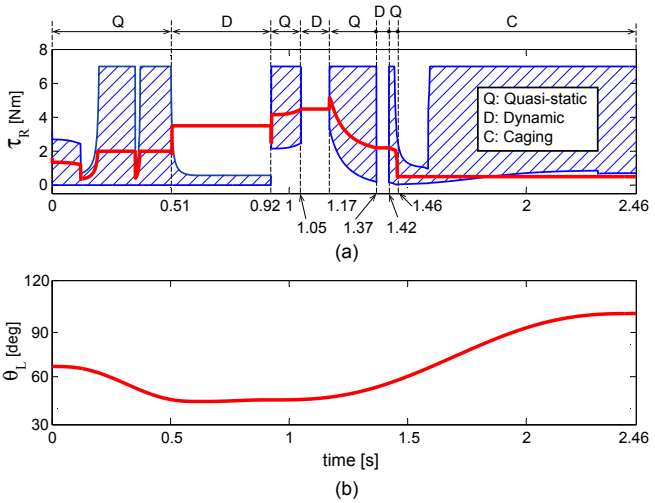

Fig. 7. Desired trajectories obtained in Phase 2. (a) Joint torque trajectory of the torque-controlled finger (right finger) and the manipulation mode. (b) Joint angle trajectory of the velocity-controlled finger (left finger).

Fig. 7(a) shows the torque trajectory of the torque-controlled finger and the manipulation mode. Let the parameters be $\tau_{margin} = 2.0$ Nm, $\tau_{caging} = 0.5$ Nm, and $\tau_{dyn} = 3.5$ Nm $(0.51 \leq t \leq 0.92$ s), 4.5 Nm $(1.05 \leq t \leq 1.17$ s), and 2.2 Nm $(1.37 \leq t \leq 1.42$ s) Nm, respectively. The applicable torque range $\mathcal{T}(\widetilde{\mu})$, which represents the intersection of the applicable joint torque range of a quasi-static manipulation for $\mu_{min} = 0$ and $\mu_{max} = 0.1$, is described by the hatched region. The grasp has force closure when the maximum torque reaches the limit of the actuator torque $\tau_{limit} = 7.0$ Nm. The solid red line is the desired torque trajectory τ_R obtained in this phase. Fig. 7(b) shows the joint angle trajectory of the velocity-controlled finger, which is obtained using a fifth-order polynomial with respect to time.

As shown in Fig. 7(a), the contact state transition with the quasi-static manipulation is impossible at $t = 0.92$ s, which corresponds to the Case 1 in Section III-B.2, when the lower right edge of the object makes contact with the link of the right finger (see #5 in Fig. 6). In order to avoid this configuration, dynamic manipulation is performed between $t = 0.51$ and 0.92 s by applying a joint torque τ_{dyn}, which exceeds the upper bound of the applicable joint torque range $\mathcal{T}(\widetilde{\mu})$. Dynamic manipulations are also performed over the two time spans when $1.05 \leq t \leq 1.17$ s and $1.37 \leq t \leq 1.42$ s, which corresponds to the Case 2 in Section III-B.2. This is because the applicable torque for the quasi-static manipulation cannot be found due to the actuator torque limit and a change in direction of the friction force, respectively. Caging manipulation is performed after $t = 1.46$ s by applying the constant joint torque τ_{caging} because the center of gravity comes across the contact normal of the vertex contacting the environment (see #8–11 in Fig. 6).

D. Experimental results and discussions

In order to verify the validity of the proposed methods, we conducted manipulation experiments. Fig. 8 shows photographs of the object and finger movements. The velocity-controlled finger is controlled by a simple PD feedback controller while the torque-controlled finger is controlled by an open-loop controller. We can see the object is moved from the initial to goal configurations as planned in Phase 2 with simple controllers.

The object starts to slide along the environment toward the right by rotating the velocity-controlled left finger clockwise while maintaining equilibrium in the quasi-static manipulation mode. The right-most contact on the environment breaks at $t = 0.51$ s by starting dynamic manipulation. By pushing the object firmly with the torque-controlled right finger, the object rotates counterclockwise around the left-most vertex contacting the environment. When the lower right edge of the object makes contact with the link of the right finger at $t = 0.92$ s, the manipulation mode is switched to the quasi-static mode. Dynamic manipulation is performed two times before caging manipulation starts at $t = 1.46$ s. Finally, the object reaches the goal configuration at $t = 2.46$ s.

The success of the proposed control strategy depends on the feasibility of dynamic manipulation. In this paper, the input joint torque, τ_{dyn}, during dynamic manipulation is determined heuristically by solving the forward dynamic problem. In our future work, we intend to develop an algorithmic approach to finding the optimal joint torque for dynamic manipulation.

The attached video shows the results of the two experiments. The first video shows the results of the experiment shown in Fig. 8, and the second video shows the results of the experiment using a regular hexagonal object having a mass of 335 g. It can be seen that the left finger breaks contact with the object several times during the caging manipulation period, which is, however, allowable in caging manipulation as long as the object is restricted by fingers within a bounded space. Accordingly, these results demonstrate the validity of the proposed control strategy that takes into account the estimated bounds of frictional coefficient.

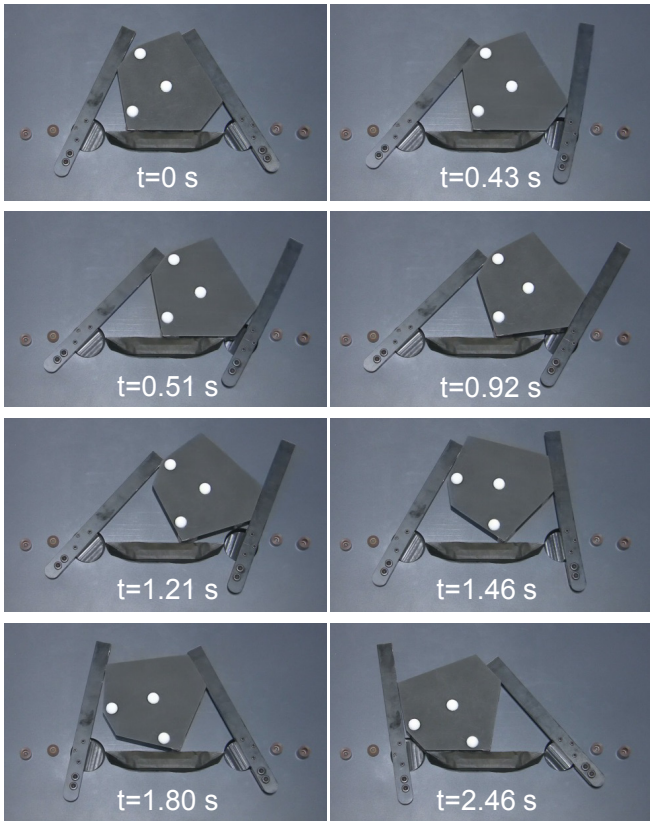

Fig. 8. Photographs of the manipulation experiment involving an asymmetric hexagonal object

V. Conclusions and future work

The present paper discussed a planning and control strategy for robotic whole-arm manipulations. The proposed control strategy can be applied to difficult conditions where not only between-body frictions exist, but also situations where quasi-static equilibrium is not always satisfied. Since it is difficult to know the coefficients of friction precisely, the present control strategy considers the estimated bounds of frictional coefficients and generates a desired trajectory that satisfies the quasi-static equilibrium over all of the estimated bounds. This is accomplished by solving the forward dynamics problem formulated as a mixed LCP in order to avoid occurring rolling contacts. When quasi-static equilibrium cannot be satisfied, manipulation is continued by switching to the dynamic manipulation mode, the validity of which is also verified by solving the forward dynamics problem.

In the future, we intend to (i) develop optimization algorithms for the contact state transition because randomized planning cannot assure the optimality of the planned transition, (ii) design control strategy in the dynamic manipulation mode in order to find optimal joint torque control inputs, and (iii) validate the proposed method for a more complicated manipulation system composed of multi-DOF fingers in a 3D space.

References

[1] M. Anitescu and F. A. Potra, “Formulating Dynamic Multi-rigid-body Contact Problems with Friction as Solvable Linear Complementarity Problems,” Nonlinear Dynamics, vol. 14, pp. 231-247, 1997.
[2] M. C. Ferris, http://pages.cs.wisc.edu/˜Ferris/path.html.
[3] K. Harada and M. Kaneko, “A Sufficient Condition for Manipulation of Envelope Family,” IEEE Trans. on Robotic and Automation, vol. 18, no. 4, pp. 597-607, 2002.
[4] J. C. Latombe, “Robot Motion Planning,” pp. 103-122, Kluwer Academic Publishers, 1996.
[5] K. M. Lynch and M. T. Mason, “Dynamic Nonprehensile Manipulation: Controllability, Planning, and Experiments, The International Journal of Robotics and Research, vol. 18, no. 1, pp. 64-92, 1999.
[6] Y. Maeda, T. Nakamura and T. Arai, “Motion Planning of Robot Fingertips for Graspless Manipulation,” Proc. of the 2004 IEEE Int. Conference on Robotics and Automation, pp. 2951-2956, 2004.
[7] H. Miyashita, T. Yamawaki and M. Yashima, “Parts Assembly by Throwing Manipulation with a One-Joint Arm,” Proc. of the 2010 IEEE/RSJ International Conference on Intelligent Robots and Systems, pp. 43-48, 2010.
[8] T. Omata and K. Nagata, “Rigid Body Analysis of the Indeterminate Grasp Force in power Grasps,” Proc. of the 1996 IEEE International Conference on Robotics and Automation, pp.1787-1794, 1996.
[9] G. A. Pereira, M. F. Campos and V. Kumar, “Decentralized Algorithms for Multi-Robot Manipulation via Caging,” The International Journal of Robotics and Research, vol. 23, no. 7/8, pp. 783-795, 2004.
[10] P. Song, M. Yashima and V. Kumar, “Dynamic Simulation for Grasping and Whole Arm Manipulation,” Proc. of the 2000 IEEE International Conference on Robotics and Automation, pp. 1082-1087, 2000.
[11] S. S. Srinivasa, M. A. Erdmann and M. T. Mason, “Control Synthesis for Dynamic Contact Manipulation,” Proc. of the 2005 IEEE International Conference on Robotics and Automation, pp. 2523-2528, 2005.
[12] D. Stewart and J. Trinkle, “An implicit time-stepping scheme for rigid-body dynamics with inelastic collisions and Coulomb friction,” Int. J. of Numerical Methods Engineering, vol. 39, pp. 2673-2691, 1996.
[13] J. C. Trinkle and J. J. Hunter, “A Framework for Planning Dexterous Manipulation,” Proc. of the 1991 IEEE International Conference on Robotics and Automation, pp.1245-1251, 1991.
[14] J. C. Trinkle, R. C. Ram, and A. O. Farahat, “Dexterous Manipulation Planning and Execution of an Enveloped Slippery Workpiece,” Proc. of the 1993 IEEE International Conference on Robotics and Automation, pp.442-448, 1993.
[15] T. Watanabe, K. Harada, T. Yoshikawa, and Z. Jiang, “Towards Whole Arm Manipulation by Contact State Transition,” Proc. of the 2006 IEEE/RSJ International Conference on Intelligent Robots and Systems, pp. 5682-5687, 2006.
[16] T. Yamawaki and M. Yashima, “Randomized Planning and Control Strategy for Whole-Arm Manipulation of a Slippery Polygonal Object,” Proc. of the 2013 IEEE/RSJ International Conference on Intelligent Robots and Systems, pp. 2485-2492, 2013.
[17] M. Yashima, Y. Shiina and H. Yamaguchi, “Randomized Manipulation Planning for A Multi-Fingered Hand by Switching Contact Modes,” Proc. of the 2003 IEEE International Conference on Robotics and Automation, pp. 2689-2694, 2003.
[18] Y. Yu and T. Yoshikawa, “Evaluation of Contact Stability between Objects,” Proc. of the 1997 IEEE International Conference on Robotics and Automation, pp. 695-702, 1997.
[19] Z. D. Wang and V. Kumar, “Object Closure and Manipulation by Multiple Cooperating Mobile Robots,” Proc. of the 2002 IEEE Int. Conference on Robotics and Automation, pp. 394-399, 2002.
[20] X. Y. Zhang, Y. Nakamura and K. Yoshimoto, “Robustness of Power Grasp,” Proc. of the 1994 IEEE International Conference on Robotics and Automation, pp.2828-2835, 1994.